



HAL
open science

Dynamic dielectric properties of isotactic polypropylene-g-maleic anhydride crosslinked by capped-end polyether diamine and filled with native or functionalized nano-graphite particles

F. Agrebi, A. Letoffé, A. Kallel, I. Royaud, Z. Ayadi, M. Ponçot, Stéphane Cuynet, Sébastien Fontana

► To cite this version:

F. Agrebi, A. Letoffé, A. Kallel, I. Royaud, Z. Ayadi, et al.. Dynamic dielectric properties of isotactic polypropylene-g-maleic anhydride crosslinked by capped-end polyether diamine and filled with native or functionalized nano-graphite particles. *Polymer Bulletin*, In press, 10.1007/s00289-022-04171-9 . hal-03813223

HAL Id: hal-03813223

<https://hal.science/hal-03813223>

Submitted on 17 Oct 2022

HAL is a multi-disciplinary open access archive for the deposit and dissemination of scientific research documents, whether they are published or not. The documents may come from teaching and research institutions in France or abroad, or from public or private research centers.

L'archive ouverte pluridisciplinaire **HAL**, est destinée au dépôt et à la diffusion de documents scientifiques de niveau recherche, publiés ou non, émanant des établissements d'enseignement et de recherche français ou étrangers, des laboratoires publics ou privés.

Metadata of the article that will be visualized in OnlineFirst

ArticleTitle	Dynamic dielectric properties of isotactic polypropylene-g-maleic anhydride crosslinked by capped-end polyether diamine and filled with native or functionalized nano-graphite particles
--------------	--

Article Sub-Title

Article CopyRight	The Author(s), under exclusive licence to Springer-Verlag GmbH Germany, part of Springer Nature (This will be the copyright line in the final PDF)
-------------------	---

Journal Name	Polymer Bulletin
--------------	------------------

Corresponding Author	FamilyName	Royaud
	Particle	
	Given Name	I.
	Suffix	
	Division	CNRS, IJL
	Organization	Université de Lorraine
	Address	54000, Nancy, France
	Division	
	Organization	Université de Lorraine, CNRS, LabEx "DAMAS"
	Address	57000, Metz, France
	Phone	
	Fax	
	Email	Isabelle.royaud@univ-lorraine.fr
URL		
ORCID	http://orcid.org/0000-0001-5469-2995	

Author	FamilyName	Agrebi
	Particle	
	Given Name	F.
	Suffix	
	Division	Faculty of Sciences of Sfax, LaMaCoP
	Organization	University of Sfax
	Address	3018, Sfax, BP, Tunisia
	Phone	
	Fax	
	Email	
	URL	
	ORCID	

Author	FamilyName	Letoffe
	Particle	
	Given Name	A.
	Suffix	
	Division	CNRS, IJL
	Organization	Université de Lorraine
	Address	54000, Nancy, France
	Division	
	Organization	Université de Lorraine, CNRS, LabEx "DAMAS"
	Address	57000, Metz, France
	Phone	
	Fax	
	Email	
URL		
ORCID		

Author	FamilyName	Kallel
	Particle	
	Given Name	A.
	Suffix	
	Division	Faculty of Sciences of Sfax, LaMaCoP
	Organization	University of Sfax
	Address	3018, Sfax, BP, Tunisia
	Phone	
	Fax	
	Email	
	URL	
	ORCID	

Author	FamilyName	Ayadi
	Particle	
	Given Name	Z.
	Suffix	
	Division	CNRS, IJL
	Organization	Université de Lorraine
	Address	54000, Nancy, France
	Phone	
	Fax	
	Email	
	URL	
	ORCID	

Author	FamilyName	Ponçot
	Particle	
	Given Name	M.
	Suffix	
	Division	CNRS, IJL
	Organization	Université de Lorraine
	Address	54000, Nancy, France
	Division	
	Organization	Université de Lorraine, CNRS, LabEx "DAMAS"
	Address	57000, Metz, France
	Phone	
	Fax	
	Email	
	URL	
	ORCID	

Author	FamilyName	Cuynet
	Particle	
	Given Name	S.
	Suffix	
	Division	CNRS, IJL
	Organization	Université de Lorraine
	Address	54000, Nancy, France
	Phone	
	Fax	
	Email	
	URL	
	ORCID	

Author	FamilyName	Fontana
	Particle	
	Given Name	S.
	Suffix	
	Division	CNRS, IJL
	Organization	Université de Lorraine
	Address	54000, Nancy, France
	Phone	
	Fax	
	Email	
	URL	
	ORCID	

Schedule	Received	2 Jan 2022
	Revised	11 Feb 2022
	Accepted	22 Feb 2022

Abstract


Dynamic dielectric properties of an isotactic polypropylene matrix grafted with maleic anhydride (CA 100) and then crosslinked by polyether amine molecules and reinforced with different weight percentages of graphite nanoplatelets (GNPs), KNG180, were studied for the first time and compared to those obtained by DMA (Dynamic Mechanical Analysis). The main objective of this work was to investigate the reinforcement effect of GNPs focusing on the GNPs/matrix interfacial adhesion using dynamic dielectric relaxation spectroscopy in the frequency range from 0.1 Hz to 1 MHz and temperature range from 20 to 140 °C. The obtained interfacial polarization increments $\Delta\epsilon_{MWS}$ from MWS (Maxwell Wagners Sillars) relaxation showed a threshold value of 3% in weight of KNG180. This analysis suggests that interfacial compatibility between matrix and fillers in the case of nanocomposite KNG180 3 wt% is higher than those of other nanocomposites. A new plasma treatment was used to modify graphite nano-fillers to produce different types of nanocomposites. The 5 wt% plasma treated graphite nanocomposite shows a good dispersion of the nano-fillers but also a high value of $\Delta\epsilon_{MWS}$, which is an indication of high graphite/graphite interaction. This evolution could show that this material can be close to the formation of an electrical percolation network.

Keywords (separated by '- ') Isotactic polypropylene - Graphite nanosheets - Dynamic dielectric properties

Footnote Information



2 **Dynamic dielectric properties of isotactic**
3 **polypropylene-g-maleic anhydride crosslinked**
4 **by capped-end polyether diamine and filled with native**
5 **or functionalized nano-graphite particles**

6 **F. Agrebi² · A. Letoffe^{1,3} · A. Kallel² · I. Royaud^{1,3}  · Z. Ayadi¹ · M. Ponçot^{1,3} ·**
7 **S. Cuynet¹ · S. Fontana¹**

8 Received: 2 January 2022 / Revised: 11 February 2022 / Accepted: 22 February 2022
9 © The Author(s), under exclusive licence to Springer-Verlag GmbH Germany, part of Springer Nature 2022

10 **Abstract**

11 Dynamic dielectric properties of an isotactic polypropylene matrix grafted with
12 maleic anhydride (CA 100) and then crosslinked by polyether amine molecules
13 and reinforced with different weight percentages of graphite nanoplatelets (GNPs), **AQ1**
14 KNG180, were studied for the first time and compared to those obtained by DMA
15 (Dynamic Mechanical Analysis). The main objective of this work was to investigate
16 the reinforcement effect of GNPs focusing on the GNPs/matrix interfacial adhesion
17 using dynamic dielectric relaxation spectroscopy in the frequency range from 0.1 Hz
18 to 1 MHz and temperature range from 20 to 140 °C. The obtained interfacial polari-
19 zation increments $\Delta\epsilon_{\text{MWS}}$ from MWS (Maxwell Wagners Sillars) relaxation showed
20 a threshold value of 3% in weight of KNG180. This analysis suggests that interfa-
21 cial compatibility between matrix and fillers in the case of nanocomposite KNG180
22 3 wt% is higher than those of other nanocomposites. A new plasma treatment was
23 used to modify graphite nano-fillers to produce different types of nanocomposites.
24 The 5 wt% plasma treated graphite nanocomposite shows a good dispersion of the
25 nano-fillers but also a high value of $\Delta\epsilon_{\text{MWS}}$, which is an indication of high graphite/
26 graphite interaction. This evolution could show that this material can be close to the
27 formation of an electrical percolation network.

28 **Keywords** Isotactic polypropylene · Graphite nanosheets · Dynamic dielectric
29 properties

A1  I. Royaud
A2 Isabelle.royaud@univ-lorraine.fr

A3 ¹ CNRS, IJL, Université de Lorraine, 54000 Nancy, France

A4 ² Faculty of Sciences of Sfax, LaMaCoP, University of Sfax, 3018 Sfax, BP, Tunisia

A5 ³ Université de Lorraine, CNRS, LabEx “DAMAS”, 57000 Metz, France

30 Introduction

31 Polypropylene (PP) is a well-known semi-crystalline thermoplastic polymer
32 which has been widely applied in many fields. Along the past two decades, PP
33 has been reinforced with several fibers to enhance its mechanical and physical
34 properties. Lately, PP/Graphite and PP/graphene composites have attracted great
35 research interest, because mechanical as well as physical properties (thermal con-
36 ductivity, electrical conductivity, barrier property, etc.) can be simultaneously
37 improved to fulfill the requirements of many practical applications [1]. The iso-
38 tactic polypropylene or iPP was mainly chosen for its mechanical properties with
39 regards to the nanocomposite conception. It is a well-known material for its prop-
40 erties and generally used in a lot of industrial application. The main advantage
41 of this nanocomposite is its capability to be used in different industrial applica-
42 tion and specifically in the automotive industry, the polymer/metal composite to
43 enlightened the structure. Composites based on isotactic polypropylene anhydride
44 (iPP-g-MAH) crosslinked by the use of polyetheramine molecules [2] were stud-
45 ied in this work as a matrix reinforced with graphite nanosheets (GNPs), KNG
46 180. Since, the use of maleic anhydride (MAH) is one of the most common ways
47 in the reactive blending to improve the interfacial adhesion in immiscible poly-
48 mer blends, particles and fibers filled polymer matrix and multi-layered multi-
49 material's composites [3].

50 The GNPs used as nano-reinforcing phase were characterized and successfully
51 dispersed into iPP-g-MAH matrix to produce iPP-g-MAH/GNPs nanocomposites.
52 In polymers and composite polymer materials, interfacial polarization is almost
53 present due to the existence of heterogeneities (multiphase systems, semi crys-
54 talline polymers, fillers, impurities). Many techniques have been used to explore
55 the interface. Among these techniques, Broadband Dielectric spectroscopy (BDS)
56 is one of the most powerful methods providing a direct experimental access to
57 a variety of physical phenomena taking place at different length and time-scale,
58 such as molecular fluctuation, charge transport processes in the bulk and at the
59 interfaces [4]. That is why in this paper, the effects of the incorporated GNPs
60 with loading of various content (1 wt%, 3 wt%, 5 wt% and 10 wt %) on the dielec-
61 tric properties of iPP-g-MAH matrix were investigated using this technique [5].

62 Experimental

63 Materials

64 The polypropylene grafted maleic anhydride used in this work is the Orevac[®] CA
65 100 from Arkema. This isotactic polypropylene is grafted with 1 wt% of maleic
66 anhydride. The maleic anhydride grafting to the iPP plays an important role in
67 two ways: First, it is well known in the literature that adding MAH to a polymer
68 such as the polypropylene can help the dispersion of a carbon-nano-filler such

69 as graphite when there is poor compatibility between the filler and the matrix.
70 PP-g-MAH was used as the nanocomposite matrix because of this reason. The
71 main problem comes from the poor mechanical behaviour of such matrix (it is
72 brittle). Thus, a crosslinked reaction that used diamine molecule and the graft
73 MAH was developed to improve the polymer mechanical behaviour and obtain
74 a ductile matrix. In this situation, the MAH helps for the homogeneous disper-
75 sion of the filler and for the crosslinking reaction used to improve the mechanical
76 properties. In the context of automotive industry and polymer/metal composite,
77 it is the adhesion then the crosslinking and then an help to the dispersion of the
78 fillers which is aimed (duality functionalization and conduction from percolation
79 of the matrix).

80 The technical specification sheet provides by Arkema indicated a yield strength
81 of 22 MPa and an elongation at break of 12% [6]. The CA 100 average molecular
82 weight is estimated at $M_n=25,000 \text{ g mol}^{-1}$ [8, 9].

83 The crosslinking agent used is the Jeffamine[®] THF 100 by huntsman [10]. It is
84 a capped-end triblock polyether diamine ($\text{H}_2\text{N-PO}_2\text{-TMO}_9\text{-PO}_3\text{-NH}_2$) and used as
85 received. It possesses a molecular weight of 1000 g mol^{-1} .

86 Two graphites were used in this work. The first one is a GNP from Knano
87 (Xianen, China) under the reference KNG 180. It presents a high carbon content
88 (> 99.5 wt%), a diameter between 8 and 100 μm and a thickness inferior to 100 nm
89 (supplier data). The second one is a KNG 180 treated by a new plasma treatment
90 developed for the exfoliation and functionalization of the graphite. The characteriza-
91 tion of those functionalized nano-fillers was already performed in a previous work
92 [11].

93 Material's preparation

94 The crosslinked material was produced with the method described in a previous arti-
95 cle [2, 6, 7]. The Jeffamine[®] THF 100 by Huntsman was used to crosslink the CA
96 100 by reactive extrusion as described in our previous work [2]. The matrix was
97 crosslinked with an amine:MAH molar ratio of 1:1. This configuration gives the best
98 mechanical properties. This material is noted CA 100 THF 100 1:1. This matrix is
99 used as reference.

100 The nanocomposites elaboration was performed at LRGP Laboratory (CNRS-
101 University of Lorraine, Nancy, France), with a 10 mm barrel extruder (Twinscrew
102 Benthop Compounding Line from Rondol Technology LdT), with a L:D ratio of
103 40:1. The rotation speed was fixed at a specific value of 20 rpm. The process is a
104 variation of the process use for the crosslinked matrix [2, 6, 7]. Figure 1 shows the
105 screw and temperature profile of the extruder.

106 A nanocomposite which can be processed at large scale using conventional
107 method for polymer processing had to be looked for (i.e., without any particu-
108 lar investment/development). In previous test, the carbon nano-fillers were added
109 early in the extrusion process but it was difficult to produce a homogeneous mate-
110 rial due to the behaviour of the filler. By introducing the fillers after the poly-
111 mer (CA 100) was completely mixed with the crosslinking agent (THF 100) in

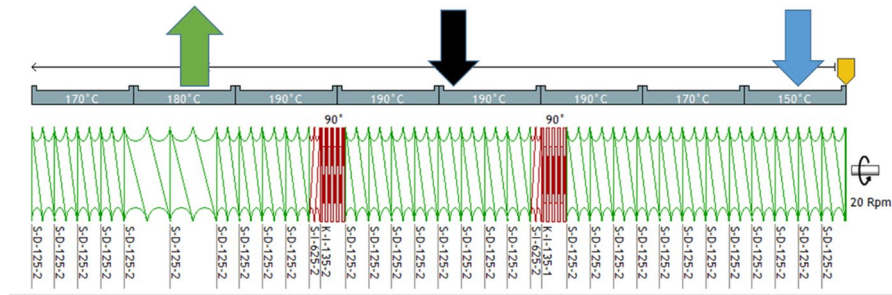


Fig. 1 Temperature and screw profile used for the nanocomposite’s elaboration. The mixing areas are in red and the conveyor element in green. The arrows indicate the introduction of the CA 100 (blue), of the crosslink agent/carbon nano-fillers (black) and the solvent extraction by vacuum pump (green)

112 a solvent (mesitylene), a better control of the filler concentration and dispersion
 113 was obtained [2]. The low screw rotation was imposed by the crosslinked reaction
 114 used in this work to produce the composite. After the introduction of the
 115 crosslinking agent in the melted CA 100, a minimum of 10 min is necessary
 116 to complete the chemical reaction. The screw rotation was calculated to obtain
 117 the optimal residence time. The CA 100 was introduced with a mass flow of
 118 1.1 g min^{-1} . The nano-fillers (KNG-180 and KNG-180 plasma treated) and the
 119 crosslinking agent (THF 100) were mixed together with mesitylene to obtain a
 120 low viscosity liquid that can be injected. The filler dispersion was obtained by
 121 a sonic bath. The mixture was injected into the extruder barrel between the two
 122 mixing areas, the mass flow rate was adapted to rich the targeted molar ratios
 123 NH_2 :MAH and nano-filler concentration. Two screw elements with large thread
 124 were added at the end of the extruder to help the mesitylene evaporation. A vac-
 125 uum pump connected to the extruder barrel and a cold trap with liquid nitrogen
 126 performed its extraction. The complete extraction of mesitylene was confirmed
 127 by FTIR spectroscopy. Two types of nanocomposite were produced. The first one
 128 with the unmodified KNG 180, with an amine:MAH molar ratio of 1:1 and a car-
 129 bon concentration of 1, 3, 5 and 10 wt%. The second type was produced with the
 130 plasma treated fillers, with a concentration of 1, 3 and 5 wt%.

131 The crosslinked matrix and the nanocomposites were shaped into 3 mm plates
 132 with injection moulding (Micro 12 cc Injection Moulding Machine/DSM Xplore).
 133 The filler concentration was confirmed by TGA analysis.

134 **Experimental procedure**

135 **SEM and TEM microscopy**

136 SEM micrographs were obtained after the samples were broken by cryofracture.
 137 The fracture pattern was examined by an environmental Quanta FEG 650 electron
 138 microscope from FEI Company. The electrons were accelerated under a tension of
 139 4 kV, under a water vapor pressure of 100 Pa.

140 Transmission electron microscopy, or TEM, was performed on an ARM-200F
 141 apparatus at an operating voltage of 200 kV. Samples were dispersed in absolute
 142 ethanol by sonication and were deposited on a copper grid and a holey carbon film.

143 Dynamic dielectric spectroscopy (DDS)

144 The dynamic dielectric spectroscopy experiments were carried out using a Novo-
 145 control System based on an Alpha Analyzer and a temperature controller (Novo-
 146 control quatro system controller BDS 1330) at the frequency range from 0.1 Hz to
 147 1 MHz and the temperature range from 20 to 140 °C on heating at a rate of 5 °C/
 148 min. The sample was fixed between two additional external electrodes of 20 mm in
 149 diameter in the sample holder and placed in a cryostat. The measured dielectric per-
 150 mittivity data were collected and evaluated by WinDETA impedance analysis soft-
 151 ware. According to the planar capacitor rule, the complex dielectric function for the
 152 polymer is expressed as [12–16]

$$153 \quad \varepsilon^*(\omega) = \varepsilon'(\omega) - j\varepsilon''(\omega) \quad (j \text{ is the square root of } -1), \quad (1)$$

154 where ε' and ε'' are the real and imaginary parts of the complex permittivity.

155 The AC conductivity of all samples has been calculated from the dielectric losses
 156 according to the relation:

$$158 \quad \sigma^*(\omega) = j\varepsilon_0\omega\varepsilon^*(\omega) = j\varepsilon_0\omega(\varepsilon' - j\varepsilon'') = \varepsilon_0\omega\varepsilon'' + j\varepsilon_0\omega\varepsilon'. \quad (2)$$

159 The real part of $\sigma^*(\omega)$ is given by

$$161 \quad \sigma_{AC}(\omega) = \varepsilon_0\omega\varepsilon''(\omega), \quad (3)$$

162 where ε_0 is the dielectric permittivity in vacuum ($8.85 \times 10^{-12} \text{ F}\cdot\text{m}^{-1}$) and ω is the
 163 angular frequency.

164 The complex dielectric permittivity can be written as a function of angular fre-
 165 quency ($\omega = 2\pi f$) in accordance with numerous possible relaxation processes
 166 caused by the mobility of different dipoles and charges in the systems and described
 167 by the Havriliak–Negami (HN) [17, 18] according to the following equation (4):

$$169 \quad \varepsilon^*(\omega) = \varepsilon_\infty + \sum_i \left[\frac{\Delta\varepsilon_i}{(1 + (j\omega\tau_{\text{HN}i})^{\alpha_i})^{\beta_i}} \right] - j \frac{\sigma_{dc}}{\varepsilon_0\omega}. \quad (4)$$

170 The parameters α_i and β_i [$0 < \alpha_i; \alpha_i\beta_i \leq 1$] define the symmetrical and asymmetri-
 171 cal broadening of the distribution of relaxation times, respectively. $\tau_{\text{HN}i}$ the char-
 172 acteristic relaxation time and $\Delta\varepsilon_i$ is the relaxation strength values. $(-j\sigma_{dc}/\varepsilon_0\omega)$ is
 173 the dc conductivity term. The index i represents the different relaxations involved in
 174 dielectric spectra.

175 Two kinds of dielectric experiments were conducted: isothermal runs with fixed
 176 temperatures and scanning frequencies and isochronal runs with fixed frequencies
 177 and varying temperature. In this work, our attention is focused on isothermal runs.
 178

179 Dynamic mechanical analysis (DMA)

180 The dynamic mechanical properties of the materials were determined using DMA
181 242C manufactured by Netzsch. Rectangular bar shaped samples of dimension
182 $20 \times 4 \times 3 \text{ mm}^3$ were machined out. The complex modulus measurement were
183 performed in three points bending mode at three different frequencies at 1 Hz
184 from $-80 \text{ }^\circ\text{C}$ to $110 \text{ }^\circ\text{C}$ and at a constant heating rate of $2 \text{ }^\circ\text{C min}^{-1}$.

185 Results and discussion

186 Scanning and transmission electronic microscopy analysis

187 SEM and TEM microscopy were performed to analyse the filler dispersion inside
188 the different nanocomposites. Figure 2 shows TEM and SEM micrographs for the
189 CA 100 THF 100 1:1 with 1 wt% of KNG 180.

190 For those materials, a good dispersion of the nano-fillers inside the polymer
191 matrix was observed with no aggregation of the graphite flakes. No debonding
192 between the graphite and the polymer was observed even after the sample prepara-
193 tion (cryofracturation). This indicates a good compatibility between the polymer and
194 the graphite. This was not expected due to the poor interaction between the polypro-
195 pylene and the graphite. The polyether diamine used to crosslink the material must
196 play an important role in the improvement of this compatibility.

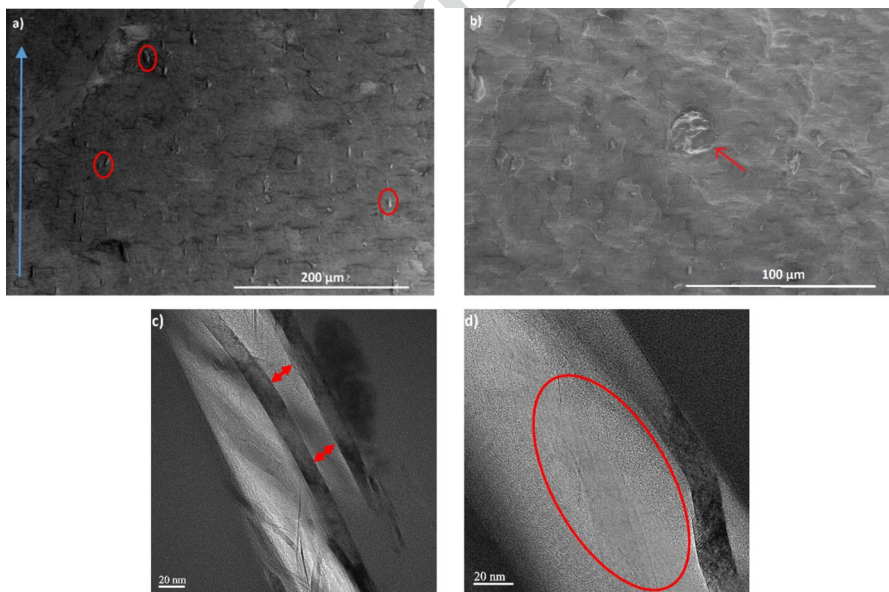


Fig. 2 SEM (a, b) and TEM (c, d) micrographs of the CA 100 THF 100 1:1 KNG-180 1 wt% nanocomposites. In a, the blue arrow indicate the injection flow direction

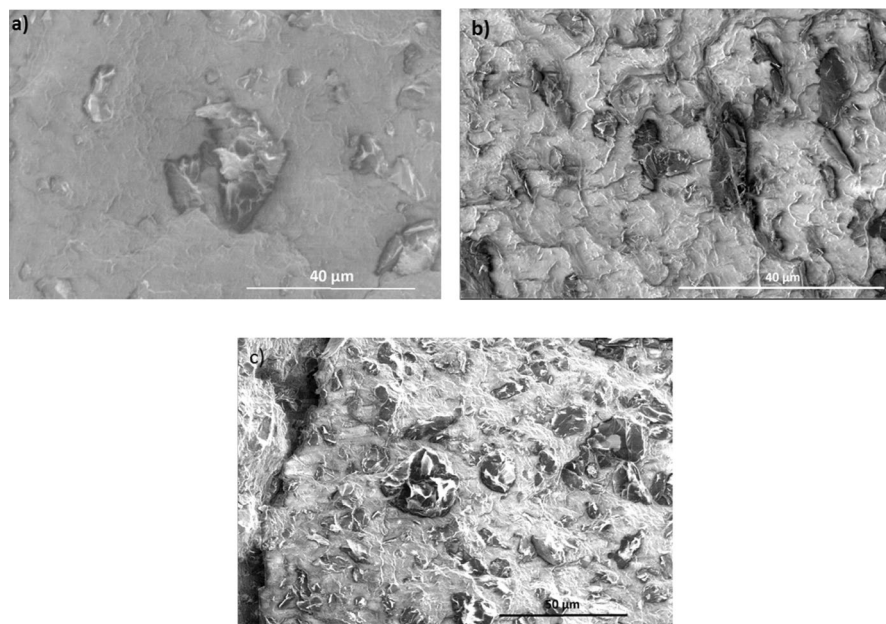


Fig. 3 SEM micrograph of the CA 100 THF 100 1:1 KNG-180 nanocomposites at 3 wt% (a), 5 wt% (b) and 10 wt% (c)

197 Figure 3 exhibits SEM micrograph for the CA 100 THF 100 1:1 filled with
198 KNG-180 at 3, 5 and 10 wt%. The nanocomposite filled at 3 wt% of KNG-180
199 shows a good dispersion of the nano-filler inside the matrix. On the contrary,
200 the nanocomposite at 5 wt% shows the formation of small aggregates, which are
201 more important at 10 wt%. The dispersion quality and polymer/carbon compat-
202 ability seem to fall for the concentration above 3 wt%.

203 Figure 4 exhibits SEM micrographs of the three nanocomposites filled with
204 plasma treated KNG-180. Like for the nanocomposites filled with untreated
205 KNG-180, the treated graphite seems to present a high adhesion to the polymer
206 matrix, with no debonding. No aggregation can be observed for the nanocompo-
207 site filled at 5 wt%. This is an important difference compared with the untreated
208 KNG-180 which implied that the functionalization of the graphite improves the
209 dispersion of the nano-fillers, hence the good polymer/carbon compatibility. This
210 behavior could be investigated by dynamic dielectric spectroscopy.

211 Figures 5 and 6 depict the comparison of the DMA signals recorded for the
212 loss factor at 1 Hz as a function of temperature for untreated and plasma treated
213 nanocomposites, respectively. All nanocomposites show the polypropylene relax-
214 ations α , β and γ [19].

215 The γ -relaxation around -40 °C related to the methyl groups motion, show low
216 amplitude variation with the filler concentration. No significant variation can be
217 observed with the type of filler or the carbon concentration.

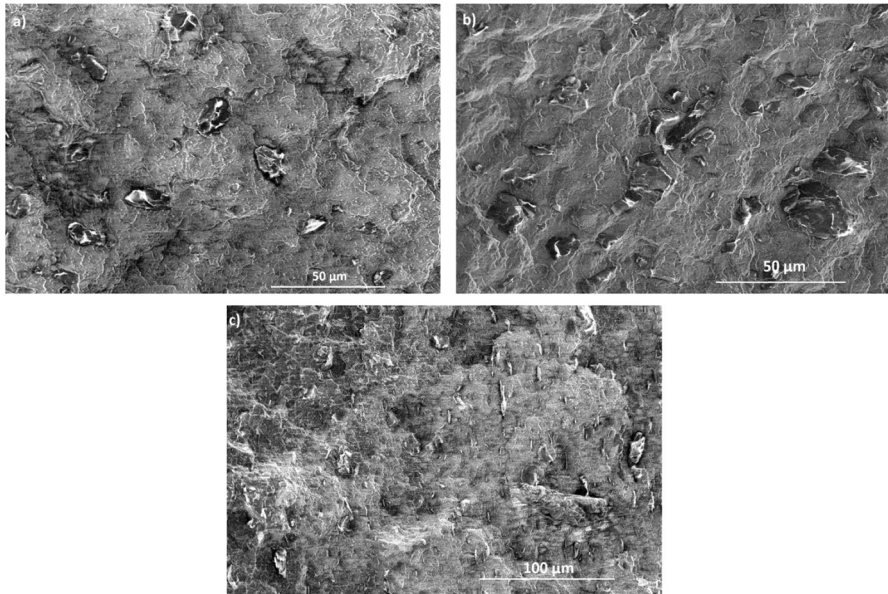


Fig. 4 SEM micrography of the CA 100 THF 100 1:1 KNG-180 plasma treated nanocomposites at 1 wt% (a), 3 wt% (b) and 5 wt% (c)

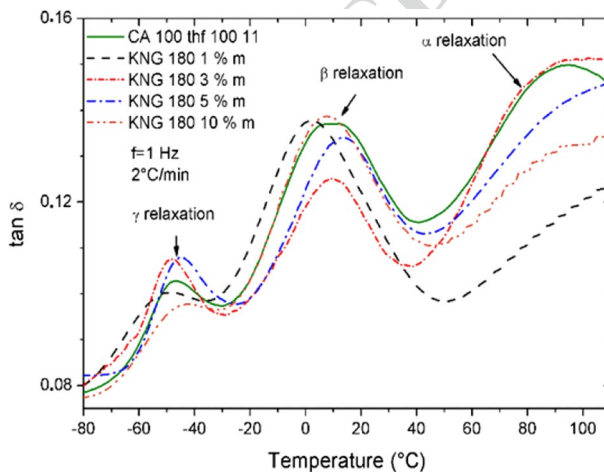


Fig. 5 Evolution of the loss factor of the CA 100 THF 100 1:1 filled with the unmodified KNG-180 between 1 and 10 wt%

218 The β -relaxation, associated to the glass transition of the polypropylene, pre-
 219 sents different amplitudes but also important variation of temperature. The initial
 220 crosslinked material, the CA 100 THF 100 1:1 exhibits a β -relaxation associated
 221 to the glass transition at 11 °C. The nanocomposite filled with 1wt% of KNG-180

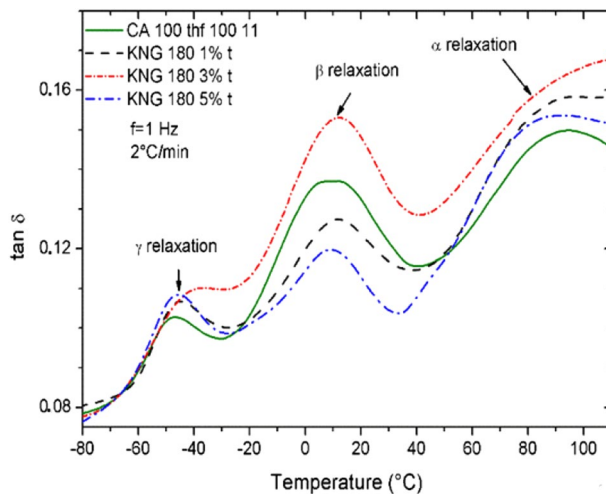


Fig. 6 Evolution of the loss factor of the CA 100 THF 100 1:1 filled with the KNG-180 plasma treated between 1 and 5 wt%

222 present a fall of the glass transition temperature to 1 °C. This temperature rises with
223 the filler content with a maximum of 14 °C at 5 wt%, and falls to 10 °C again at 10
224 wt%. The nano-fillers seem to affect the amorphous chains mobility depending on
225 the carbon concentration. The first fall could be explained by a degradation of the
226 crosslinking network by the carbon filler. On the opposite, the rise observed between
227 1 wt% and 5 wt% of carbon filler shows that the KNG-180 impacts the polypropyl-
228 ene macromolecular chains mobility. These results are in with the literature on the
229 nanocomposite elaboration [20, 21]. The final fall, between 5 and 10 wt%, can be
230 linked to the formation of the aggregate of the filler inside the matrix and the disper-
231 sion then the degradation. On the opposite, the nanocomposite filled with the KNG-
232 180 plasma treated shows a small rise of its glass transition temperature, from 12 °C
233 at 1 wt%, to 13 °C at 3 and 5 wt%. This evolution, different from the untreated fillers
234 materials, can be explained by a higher compatibility between the polymer and the
235 filler and a better dispersion as observed by SEM and TEM microscopy.

236 Finally, the α -relaxation, associated to local motions within the crystalline phase
237 is located around 90 °C for the nanocomposites. The relaxation amplitudes exhibit
238 an important variation that could be explained by the crystalline phase evolution and
239 the possible transcrystallinity on the graphite surface.

240 **Dynamic dielectric analysis studies**

241 **CA 100 matrix**

242 Figure 7 shows the real and imaginary parts of the complex permittivity versus fre-
243 quency, for the matrix isotactic polypropylene grafted with maleic anhydride CA
244 100 THF 100 crosslinked in ratio 1:1 (noted CA 100 THF 100 1:1).

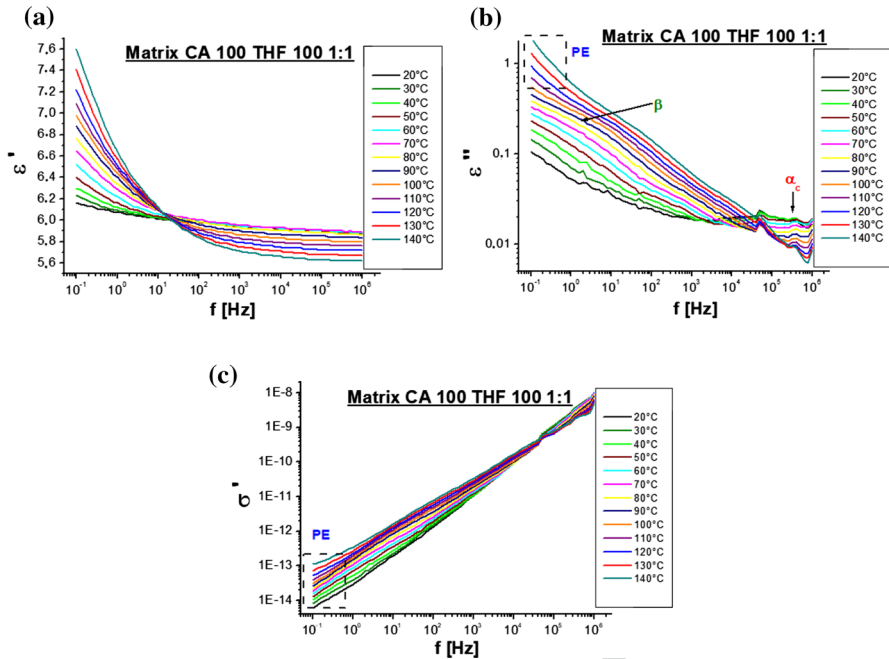


Fig. 7 Frequency dependence of (a) ϵ' , (b) ϵ'' and (c) σ_{ac} for the matrix CA 100 THF 100 1:1 at the temperature region [20–140 °C]

245 ϵ' is related to the number of dipoles which re-orient in the electric field, thus
 246 when the temperature is varied, the signal is changing drastically when the different
 247 relaxations occur in the material under study (i.e., polypropylene grafted MAH and
 248 crosslinked macromolecular chains).

249 Three relaxation phenomena can be observed. The first one appears between 10^3
 250 Hz and 1 MHz, which could be ascribed to the α_c relaxation related to the crystal-
 251 line phase [22]. The PP grafted with maleic anhydride presented higher crystallin-
 252 ity percentages than did the pure PP. The increase in the percentage of crystallinity
 253 was ascribed to the reduction in molecular weight and to the rise of polarity of
 254 the grafted samples [23]. The second relaxation process is observed around 10^2 Hz
 255 which can be ascribed to the sub-glass transition relaxation (β -relaxation) [24], and
 256 is related to the presence of polar maleic anhydride/amide/imide groups present
 257 in the polymer [25]. These two relaxations are also observed in DMA analysis [2]
 258 (Figs. 5, 6). The third relaxation, the γ relaxation associated with the movements
 259 of the methyl groups of the polypropylene chain appears only at lower temperature
 260 range (around -50°C) and cannot be observed here. Due to the important differ-
 261 ence between the two experimental methods, the temperatures and amplitudes asso-
 262 ciated to the different relaxations shows important variations, and make the compar-
 263 ison difficult. The DMA seem more appropriate to analyses the small variation of
 264 the relaxation temperature such as the β -relaxation associated with the glass transi-
 265 tion, but the dielectric spectroscopy allow an analysis at high frequency. In addition,

266 the MWS relaxation localized at the interface between the polymer and the matrix
 267 that will be used to describe the nanocomposite cannot be observed by DMA.

268 No important differences between the electrical or dielectrical property of iso-
 269 tactic, atactic and syndiotactic polypropylene are expected. Some differences can be
 270 found in the capacity of the dipoles to re-orient in the electrical field if the poly-
 271 mer is crystalline (isotactic and syndiotactic) compared to a more amorphous atactic
 272 polypropylene but these slight differences would not be seen at the interfaces with
 273 the graphite filler when observing the MWS relaxation.

274 Another special feature, ascribed to the electrode polarization (EP), can be
 275 detected from Fig. 7 by a large dispersion of ϵ' ($\Delta\epsilon \gg 1$) in low frequency region.
 276 Such mechanism is detected again on the variation of the electrical conductivity σ_{ac}
 277 versus frequency (see Fig. 7c) by a significant decrease of σ_{ac} in low frequencies
 278 below the plateau region which, therefore, tends to be superimposed on the dc bulk
 279 conductivity (σ_{dc}) [4].

280 Nanocomposites with untreated KNG180

281 The addition of GNPs into CA 100 THF 100 1:1 matrix increases the dielectric
 282 losses and generates other relaxation processes, directly related to the fillers, accord-
 283 ing to Fig. 8.

284 The crystalline peak α_c is found to be at about the same temperature with a higher
 285 intensity and correspondingly larger area. Moreover, an additional process appears
 286 at higher temperature and is ascribed to the interfacial polarization known as the
 287 Maxwell–Wagner–Sillars (MWS) effect. This relaxation arises from the accumula-
 288 tion of charge carriers at the interfaces between the GNPs and CA 100 THF 100 1:1
 289 matrix deriving a more or less conductive material depending on the nature, size and
 290 the volume fraction of the filler.

291 Table 1 presents the interfacial dielectric increments or polarization intensities
 292 $\Delta\epsilon_{MWS}$, defined by $\Delta\epsilon_{MWS} = \epsilon_s - \epsilon_\infty$ [26, 27] and deduced by fitting curves using
 293 the following Havriliak–Negami (HN) function:

$$294 \quad \epsilon'' = \sum_i \left[\frac{\Delta\epsilon_i \sin\beta\varphi}{\left[1 + 2(\omega\tau_{HNi})^{\alpha_i} \cos\left(\alpha_i \frac{\pi}{2}\right) + (\omega\tau_{HNi})^{2\alpha_i} \right]^{\frac{\beta_i}{2}}} \right] + j \times \frac{\sigma_{dc}}{\epsilon_0\omega}, \quad (5)$$

$$295 \quad \text{With, } \varphi = \arctan \frac{(\omega\tau)^\alpha \sin\left(\alpha \frac{\pi}{2}\right)}{1 + (\omega\tau)^\alpha \cos\left(\alpha \frac{\pi}{2}\right)} \text{ and } \tau_{\max,\epsilon} = \tau_{HN} \left[\frac{\sin\left(\frac{\alpha\beta\pi}{2+2\beta}\right)}{\sin\left(\frac{\alpha\pi}{2+2\beta}\right)} \right]^{\frac{1}{\alpha}}. \quad (6)$$

297 One example of the fitting procedure with a separation of overlapping relaxation
 298 regions via the deconvolution of ϵ'' at 130 °C and between 0.1 Hz and 10^4 Hz is
 299 shown in Fig. 9 for all nanocomposites.
 300

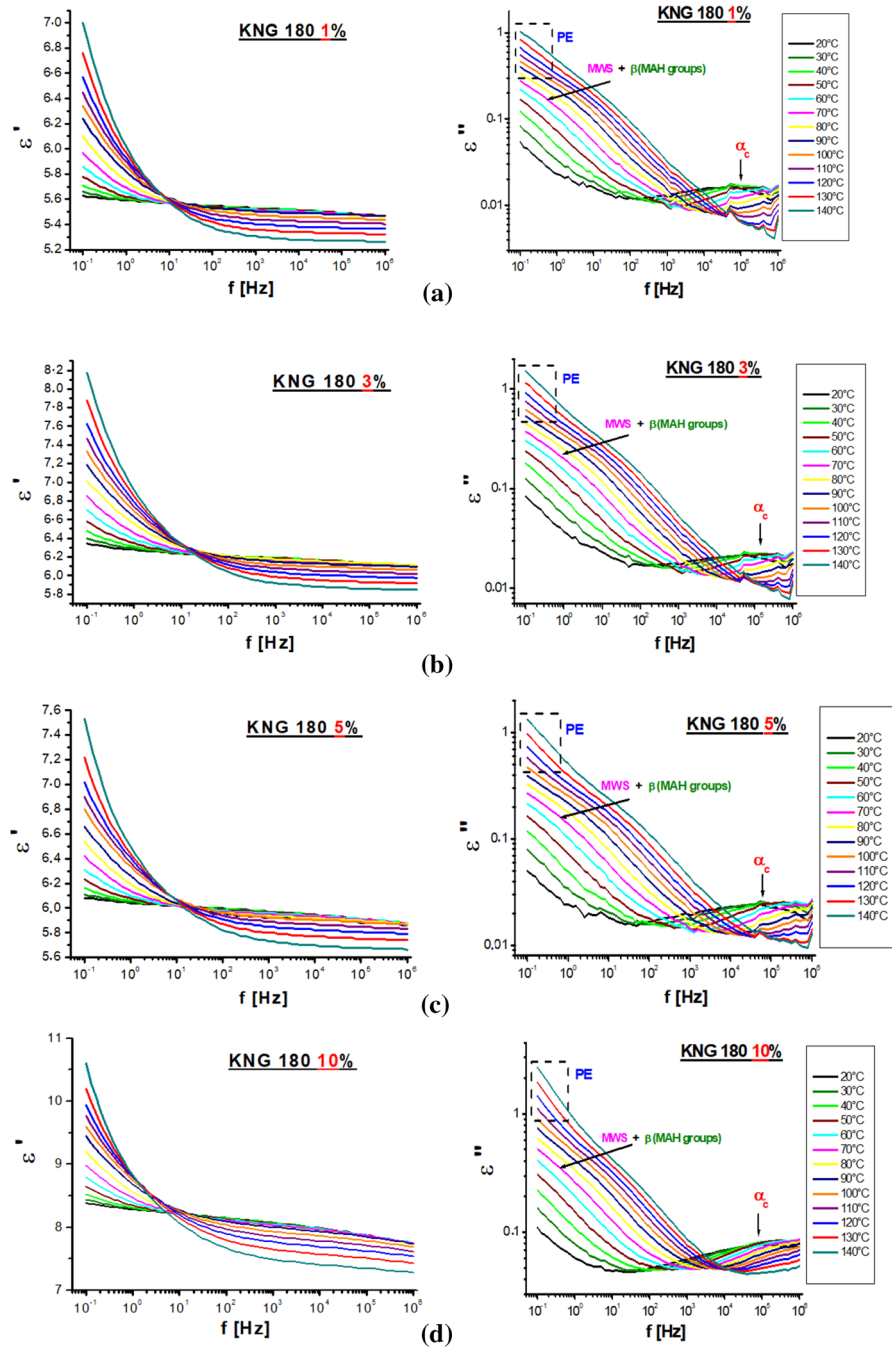


Fig. 8 Frequency dependence of ϵ' and ϵ'' for the nanocomposites KNG-180 **a** 1%, **b** 3%, **c** 5% and **d** 10% at the temperature region [20–140 °C]

Table 1 MWS polarization dielectric increments for all unmodified nanocomposites

	$\Delta\epsilon_{MWS}$ (1801m%)	$\Delta\epsilon_{MWS}$ (1803m%)	$\Delta\epsilon_{MWS}$ (1805m%)	$\Delta\epsilon_{MWS}$ (18010m%)
100 °C	0.24	0.18	0.26	0.27
110 °C	0.27	0.19	0.29	0.32
120 °C	0.28	0.26	0.32	0.35
130 °C	0.35	0.34	0.39	0.42
140 °C	0.40	0.39	0.43	0.54

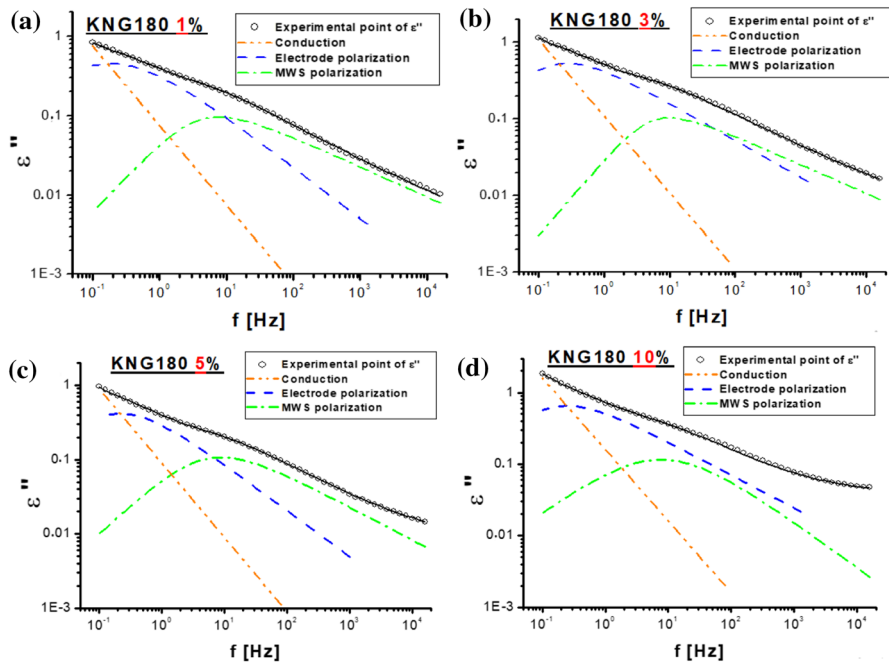


Fig. 9 Imaginary part of ϵ'' versus frequency for nanocomposites **a** KNG-180 1%, **b** KNG-180 3%, **c** KNG-180 5% and **d** KNG-180 10% at 130 °C and between 0.1 and 10⁴ Hz. Solid lines indicate the fit by Havriliak–Negami model (Eq. 4) and dashed lines indicate the deconvolution of ϵ'' according to different processes

301 It is clear, from Table 1, that $\Delta\epsilon_{MWS}$ increased with the temperature. This phe-
 302 nomenon is due to the greatest number of free charges, which can migrate and then
 303 block towards the GNPs/CA 100 THF 100 1:1 matrix interfaces. In general, it is
 304 noted that a rise in the temperature leads to an increase in the relaxation accompa-
 305 nished with shift of the maximum towards the high frequencies suggesting that the
 306 aptitude of the charge carriers to be polarized at the interface is more important at
 307 high temperatures [4, 28].

308 Furthermore, the variation of the interfacial polarization intensities gives us
 309 an idea about both types of interactions filler–filler and filler–matrix [29]. As it
 310 can be seen, the interfacial polarization intensities $\Delta\epsilon_{MWS}$ showed a threshold

311 value of 3% in weight of KNG-180. Variations were explained with attractive
 312 and repulsive GNPs–GNPs and GNPs–CA 100 THF 100 1:1 matrix interaction.
 313 A decrease in MWS polarization intensity with the increase of the reinforcement
 314 (from 1 wt% to 3 wt% of KNG-180) (see Table 1) can be noted. This is explained
 315 by a better adhesion between the reinforcement and the matrix indicating a rigidi-
 316 fication of the GNPs–CA 100 THF 100 1:1 matrix interfacial region which in turn
 317 reduced the ability of dipole to relax. This result is in good agreement with DMA
 318 analysis. Incorporating higher KNG-180 content (5 wt% and 10 wt% of GNPs)
 319 leads to reduce their mutual distances and interactions between GNPs start to
 320 occur, in good coherence with SEM and TEM, which enhances the formation of
 321 small aggregates. These interactions become stronger than those of GNPs–matrix
 322 (see Fig. 4). In fact, increases in the polarization intensity are interpreted with
 323 repulsive interactions between the CA 100 THF 100 1:1 matrix and GNPs. How-
 324 ever, decreases in the polarization intensity are explained with high attractive
 325 GNPs–GNPs interactions and predominately GNPs–matrix interactions. In this
 326 case, the better distribution of the GNPs reduces agglomeration and increases the
 327 reinforcement effect of GNPs (see Fig. 10).

328 In view of that, the properties of polymer nanocomposites largely depend on the
 329 dispersion and distribution of nanofillers within the matrix, the filler–polymer com-
 330 patibility and their interfacial interaction, the nanofiller content should be, therefore,
 331 carefully chosen to have better properties. In this case, it can be concluded that the
 332 nanocomposite with 3% of GNPs (KNG 180 3%) has the best rigidity given their
 333 low value of $\Delta\epsilon_{MWS}$ compared to other nanocomposites. The same result is shown
 334 by the mechanical study. Thus, the addition of a high reinforcement rate (3% of
 335 KNG-180) does not seem to be a solution to have the good reinforcement–matrix
 336 adhesion. To overcome this problem, plasma treatment of GNPs was intended.

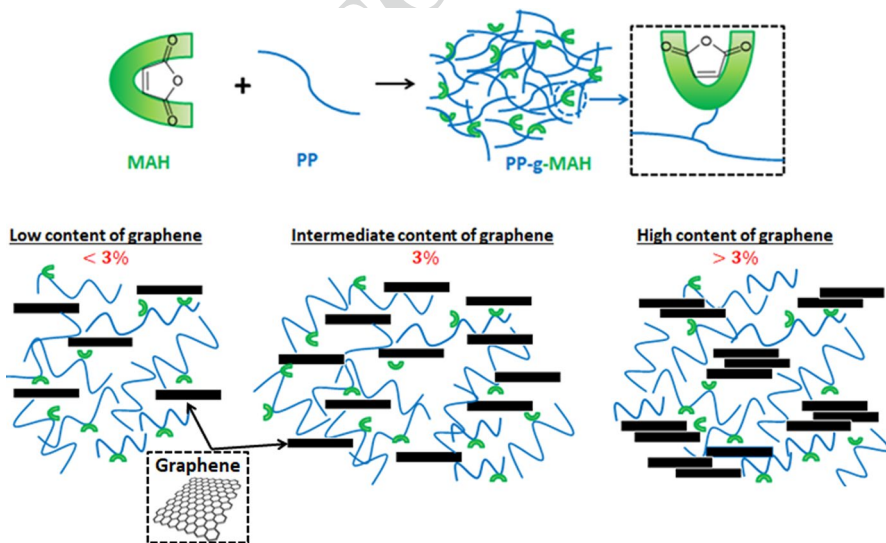


Fig. 10 Schematic illustration of GNPs/GNPs and GNPs/matrix interactions

337 In general, oxygen plasma treatment was employed to conduct the surface func-
 338 tionalization of GNPs by grafting the considerable oxygen-functional groups but
 339 without noticeably damaging the structure of graphene. In [30] authors found that
 340 the plasma-treated GNPs exhibited an enhanced electrostatic affinity with Cu pow-
 341 der, resulting in the P-GNP/Cu composite with a uniform GNPs distribution and
 342 a good interfacial bonding. Therefore, they concluded that this treatment provides
 343 a general and effective strategy to improve graphene distribution and mechanical
 344 properties of graphene/metal composites compared with the untreated composites.

345 The next section describes the dielectric results obtained for plasma-treated
 346 KNG180.

347 Nanocomposites with plasma-treated KNG-180

348 Most previous studies were focused on fiber–surface treatment methods and the
 349 resultant effects on the physical, dielectric, and mechanical properties of different
 350 fiber–matrix composite systems. The improvement of dielectric properties as well as
 351 mechanical study of composites mainly depends on (i) size effect and (ii) charge dis-
 352 tribution between the inclusions and the matrix, (iii) the large surface area of inclu-
 353 sions, which creates large interaction with the matrix and (iv) changing the polymer
 354 morphology due to the surface of inclusions [31]. In this section, as said before, this
 355 paper described the study of the relationship between surface modification of GNPs
 356 via plasma treatment and the GNPs/matrix interactions.

357 Figure 11 shows the real and imaginary parts of the complex permittivity versus
 358 frequency, for the nanocomposites KNG-180 1% with plasma-treated GNPs. Like-
 359 wise, to untreated KNG-180, the dielectric analyses of treated KNG-180 shows the
 360 presence of the α_c relaxation related to the crystalline phase, the sub-glass transi-
 361 tion relaxation (β -relaxation), the MWS interfacial polarization and the electrode
 362 polarization.

363 From Fig. 12, the impact of plasma treatment on the dielectric responses of the
 364 KNG-180 (from 1 to 5%) nanocomposites is manifested.

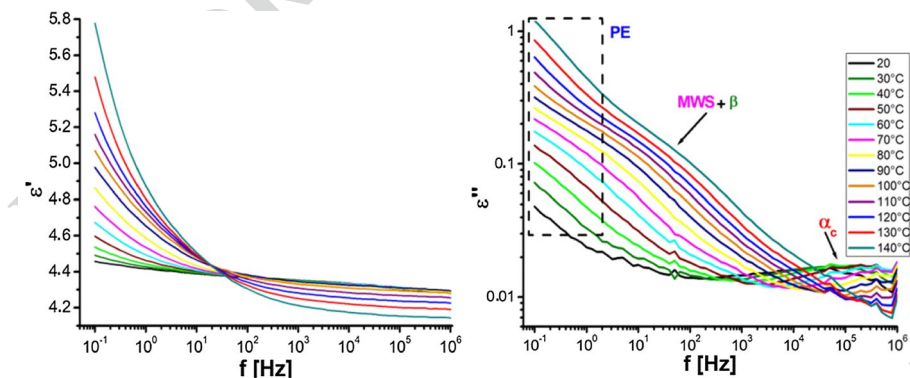


Fig. 11 Frequency dependence of ϵ' and ϵ'' for the plasma-treated nanocomposites KNG-180 1% at the temperature region [20–140 °C]

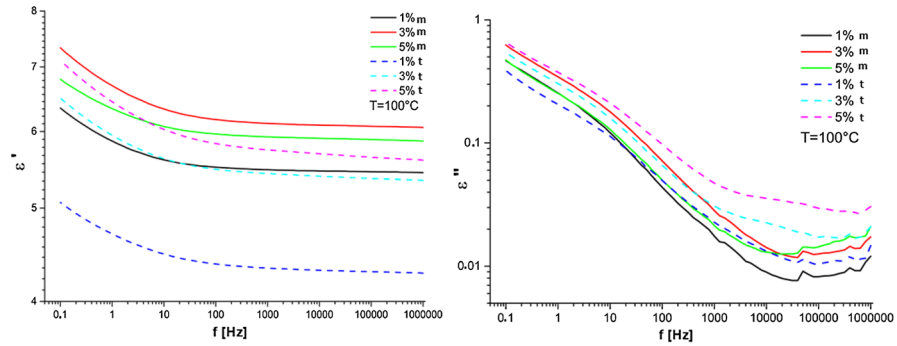


Fig. 12 Frequency dependence of ϵ' and ϵ'' for the untreated and the plasma-treated nanocomposites KNG-180 1%, KNG-180 3% and KNG-180 5% at 100 °C

365 As observed, an increase in ϵ' is much more significant for the untreated nano-
 366 composites compared to the treated ones. It is possible to explain such behaviour
 367 by evaluating the interfacial polarization intensities $\Delta\epsilon_{MWS}$ for both untreated and
 368 treated nanocomposites (see Table 2).

369 Similar to untreated nanocomposites, an increase of $\Delta\epsilon_{MWS}$ can be noted with
 370 the temperature for all the treated nanocomposites for the same reason [4, 28].

371 In addition, a difference in the value of $\Delta\epsilon_{MWS}$ between untreated and treated
 372 nanocomposites can be noticed. In fact, untreated nanocomposites show the high-
 373 est values of $\Delta\epsilon_{MWS}$ for 1% and 3% of GNPs and the lowest values for 5% of
 374 GNPs compared to treated nanocomposites.

375 The plasma treatment of GNPs was performed to exfoliate, functionalized the
 376 graphite structure and have good bonding between GNP and matrix GNPs–matrix
 377 and, therefore, getting a composite with good mechanical performance. Those
 378 result found in the case of plasma treated KNG180 5% is not expected. The
 379 increase of $\Delta\epsilon_{MWS}$ indicates not only the significant degradation of GNPs–matrix
 380 interactions, but also a significant increase in GNPs–GNPs interactions. As the
 381 obtained ATG and DRX results, as well as the SEM and TEM observations,
 382 did not show any degradation in the dispersion of GNPs between 3 and 5% of
 383 GNPs, it is more consistent to associate this evolution with the greatest inter-
 384 action between GNPs. This can be explained by the fact that the plasma treat-
 385 ment has reduced the thickness of the GNPs, they can be distributed more evenly
 386 within the matrix, reducing the distance between the GNPs and increasing their
 387 interaction.

388 However, a decrease of $\Delta\epsilon_{MWS}$ is detected for the treated KNG180 1% and
 389 KNG180 3%. The plasma treatment leads to these nanocomposites showing signifi-
 390 cantly improved interfacial bonding as compared to untreated ones. Those results
 391 were in good agreement with the DMA analysis. On the contrary to Wenying Zhou
 392 et al. [32] this system is not a percolative polymer nanocomposite and this system
 393 is not concerned with intra-particle polarization but only inter-particle polarization
 394 and interaction between the macromolecular chain of the matrix and the graphite
 395 nanofillers.

Table 2 MWS polarization intensities for untreated and plasma treated nanocomposites

	$\Delta\epsilon_{MWS}$ (1801m%)	$\Delta\epsilon_{MWS}$ (1801f%)	$\Delta\epsilon_{MWS}$ (1803m%)	$\Delta\epsilon_{MWS}$ (1803f%)	$\Delta\epsilon_{MWS}$ (1805m%)	$\Delta\epsilon_{MWS}$ (1805f%)
100 °C	0.24	0.19	0.18	0.10	0.26	0.46
110 °C	0.27	0.20	0.19	0.12	0.29	0.49
120 °C	0.28	0.22	0.26	0.13	0.32	0.51
130 °C	0.35	0.29	0.34	0.15	0.39	0.39
140 °C	0.40	0.35	0.39	0.19	0.43	0.43

396 Conclusions

397 In this work, a new plasma treatment [10] was used to modify a graphite nano-
398 filler to produce two types of nanocomposites. The two fillers exhibit variations
399 of thickness and surface functionalization as shown before. The polymer matrix
400 used was a PP-g-MAH crosslinked with polyether amine molecules. Both nano-
401 composites were produced by twin-screw reactive extrusion [6]. The nanocom-
402 posite characterization exhibits important variation of the fillers dispersion inside
403 the crosslinked polymer depending of the fillers concentration and functionali-
404 zation, with a rise of the dispersion quality with the plasma treatment and the
405 absence of aggregation at 5 wt%.

406 The nanocomposite characterization by DMA shows the polypropylene classic
407 relaxational phenomena (α -, β - and γ -relaxations) but the temperature associated
408 to those relaxations remains close for the different fillers and carbon concentra-
409 tions [2, 6]. In addition, as no information can be obtained by DMA on the graph-
410 ite/polymer interphase; it was thus necessary to analyze the fillers/polymer inter-
411 actions with dynamical dielectric spectroscopy.

412 In this paper, it was shown that Dynamical dielectric spectroscopy results exhibit
413 an additional process, the interfacial polarization known as the Maxwell–Wag-
414 ner–Sillars (MWS) effect that can be used to characterize the polymer/filler inter-
415 phases. The interfacial polarization increments $\Delta\epsilon_{MWS}$ calculated from the MWS
416 relaxation can be correlated with the fillers dispersion observed by SEM and TEM
417 microscopies. This can be used as a new way to analyse the Graphite/polymer and
418 Graphite/graphite interaction inside the nanocomposite. The 5 wt% treated graphite
419 nanocomposite shows an interesting evolution. This nanocomposite exhibits a good
420 dispersion of the nano-fillers but also a high value of $\Delta\epsilon_{MWS}$, which is an indication
421 of high graphite/graphite interaction. This evolution could indicate that this material
422 can be close to the formation of an electrical percolation network.

423 **Acknowledgements** The authors thank S. Migot and J. Ghanbaja (CC3M, Jean Lamour Institute) for
424 TEM analysis and the collaborators C. Hérold, G. Henrion and C. Noel for the GNP plasma treatment
425 from IJL and S. Hoppe for the reactive extrusion process from LRGP. This work was partially supported
426 by the internal and strategical project CoPoGraF of the Jean Lamour Institute and by a MESR grant of the
427 French government.

428 References

- 429 1. Wang D, Zhang X, Zha J et al (2013) Dielectric properties of reduced graphene oxide/polypropy-
430 lene composites with ultralow percolation threshold. *Polymer* 54:1916–1922. [https://doi.org/](https://doi.org/10.1016/j.polymer.2013.02.012)
431 [10.1016/j.polymer.2013.02.012](https://doi.org/10.1016/j.polymer.2013.02.012)
- 432 2. Létoffé A, García-Rodríguez SM, Hoppe S et al (2019) Switching from brittle to ductile isotactic
433 polypropylene-g-maleic anhydride by crosslinking with capped-end polyether diamine. *Polymer*
434 164:67–78. <https://doi.org/10.1016/j.polymer.2019.01.015>
- 435 3. Ha C, Cho Y, Go J et al (2000) Dynamic mechanical properties of polypropylene-g-maleic anhy-
436 dride and ethylene-propylene-diene terpolymer blends: effect of blend preparation methods. *J*
437 *Appl Polym Sci* 77:2777–2784. [https://doi.org/10.1002/1097-4628\(20000919\)77:12](https://doi.org/10.1002/1097-4628(20000919)77:12)

- 438 4. Agrebi F, Ghorbel N, Ladhar A et al (2017) Enhanced dielectric properties induced by loading
439 cellulosic nanowhiskers in natural rubber: Modeling and analysis of electrode polarization.
440 Mater Chem Phys 200:155–163. <https://doi.org/10.1016/j.matchemphys.2017.06.058>
- 441 5. Rekik H, Ghallabi Z, Royaud I et al (2013) Dielectric relaxation behaviour in semi-crystalline poly-
442 vinylidene fluoride (PVDF)/TiO₂ nanocomposites. Compos Part B 45:1199–1206. [https://doi.org/](https://doi.org/10.1016/j.compositesb.2012.08.002)
443 [10.1016/j.compositesb.2012.08.002](https://doi.org/10.1016/j.compositesb.2012.08.002)
- 444 6. Létoffé A, Hoppe S, Lainé R et al (2019) Resilience improvement of an isotactic polypropylene-g
445 maleic anhydride by crosslinking using polyether triamine agents. Polymer 179:121655. [https://doi.](https://doi.org/10.1016/j.polymer.2019.121655)
446 [org/10.1016/j.polymer.2019.121655](https://doi.org/10.1016/j.polymer.2019.121655)
- 447 7. Lara A, Létoffé A, Hoppe S et al (2020) Elaboration and characterization of an isotactic polypropy-
448 lene-g-maleic anhydride crosslinked by a bis(amino)-calix[4]arene derivative. J Appl Polym Sci
449 138:49889. <https://doi.org/10.1002/app.49889>
- 450 8. Novais RM, Covas JA, Paiva MC (2012) The effect of flow type and chemical functionalization
451 on the dispersion of carbon nanofiber agglomerates in polypropylene. Compos Part A 43:833–841.
452 <https://doi.org/10.1016/j.compositesa.2012.01.017>
- 453 9. Butylina S, Hyvärinen M, Kärki T (2012) A study of surface changes of wood-polypropylene com-
454 posites as the result of exterior weathering. Polymer Degradation stability 97:337–345. [https://doi.](https://doi.org/10.1016/j.polyimdegradstab.2011.12.014)
455 [org/10.1016/j.polyimdegradstab.2011.12.014](https://doi.org/10.1016/j.polyimdegradstab.2011.12.014)
- 456 10. Jeffamines® Polyetheramines, Technical Specifications Sheet by Hunstman.
- 457 11. Létoffé A, Cuynet S, Noel C et al (2021) Functionalisation and exfoliation of a nano-graphite with
458 low temperature pulse plasma in distilled water. Phys Chem Chem Phys (submitted, under review) **AQ2**
- 459 12. Ozkazanc E, Zor S, Ozkazanc H et al (2012) Synthesis, characterization and dielectric behavior of
460 (ES)-form polyaniline/cerium(III)-nitrate-hexahydrate composites. Mater Chem Phys 133:356–362.
461 <https://doi.org/10.1016/j.matchemphys.2012.01.037>
- 462 13. Sarkar A, Ghosh P, Meikap AK et al (2008) Electrical-transport properties of iodine-doped conduct-
463 ing polyaniline. J Appl Polym Sci 108:2312. <https://doi.org/10.1002/app.27615>
- 464 14. Qi YN, Xu F, Ma HJ et al (2008) Thermal stability and glass transition behavior of PANI/MWNT
465 composites. J Therm Anal Calorim 91:219. <https://doi.org/10.1007/s10973-008-8978-2>
- 466 15. Arous M, Ben Amor I, Boufi S et al (2007) Experimental study on dielectric relaxation in alfa fiber
467 reinforced epoxy composites. J Appl Polym Sci 106:3631–3640. <https://doi.org/10.1002/app.26885>
- 468 16. Ladhar A, Arous M, Kaddami H et al (2014) Molecular dynamics of nanocomposites natural rub-
469 ber/cellulose nanowhiskers investigated by impedance spectroscopy. J Mol Liq 196:187–191.
470 <https://doi.org/10.1016/j.molliq.2014.03.040>
- 471 17. Addiego F, Dahoun A, G'Sell C et al (2006) Characterization of volume strain at large deformation
472 under uniaxial tension in high-density polyethylene. Polymer 47:4387–4399. [https://doi.org/10.](https://doi.org/10.1016/j.polymer.2006.03.093)
473 [1016/j.polymer.2006.03.093](https://doi.org/10.1016/j.polymer.2006.03.093)
- 474 18. Potts JR, Dreyer DR, Bielawski CW et al (2011) Graphene-based polymer nanocomposites. Polymer
475 52:5–25. <https://doi.org/10.1016/j.polymer.2010.11.042>
- 476 19. Gulrez SKH, Mohsin MEA, Shaikh H et al (2013) A review on electrically conductive polypropyl-
477 ene and polyethylene. Polym Compos 35:900–914. <https://doi.org/10.1002/pc.22734>
- 478 20. Havriliak S, Negami S (1966) A complex plane analysis of a-dispersions in some polymer systems.
479 J Polym Sci Part C 14:99–117. <https://doi.org/10.1002/polc.5070140111>
- 480 21. Havriliak S, Negami S (1967) A complex plane representation of dielectric and mechanical relaxa-
481 tion processes in some polymers. Polymer 8:161–210. [https://doi.org/10.1016/0032-3861\(67\)](https://doi.org/10.1016/0032-3861(67)90021-3)
482 [90021-3](https://doi.org/10.1016/0032-3861(67)90021-3)
- 483 22. Ridhore A, Jog JP (2012) A dynamic mechanical and dielectric relaxation study of PP-g-MAH/ clay
484 nanocomposites. Open Macromol J 6:53–58. <https://doi.org/10.2174/1874343901206010053>
- 485 23. Bettini SHP, Agnelli JAM (2002) Grafting of maleic anhydride onto polypropylene by reactive
486 extrusion. J Appl Polym Sci 85:2706–2717. <https://doi.org/10.1002/app.10705>
- 487 24. Motori A, Montanari G, Saccani A et al (2007) Electrical conductivity and polarization processes
488 in nanocomposites based on isotactic polypropylene and modified synthetic clay. J Polym Sci Part B
489 Polym Phys 45:705–713. <https://doi.org/10.1002/polb.21091>
- 490 25. Bohning M, Goering H, Fritz A et al (2005) Dielectric study of molecular mobility in poly (propyl-
491 ene-graft-maleic anhydride)/clay nanocomposites. Macromolecules 38:2764–2774. [https://doi.org/](https://doi.org/10.1021/ma048315c)
492 [10.1021/ma048315c](https://doi.org/10.1021/ma048315c)
- 493 26. Jin X, Zhang S, Runt J (2002) Observation of a fast dielectric relaxation in, semicrystalline
494 poly(ethylene oxide). Polymer 43:6247–6254. [https://doi.org/10.1016/S0032-3861\(02\)00560-8](https://doi.org/10.1016/S0032-3861(02)00560-8)

- 495 27. Havriliak S, Havriliak SJ (1996) Comparison of the Havriliak-Negami and stretched exponential
496 functions. *Polymer* 37:4107–4110. [https://doi.org/10.1016/0032-3861\(96\)00274-1](https://doi.org/10.1016/0032-3861(96)00274-1)
497
- 498 28. Triki A, Guicha M, Ben Hassen M et al (2011) Studies of dielectric relaxation in natural fibres rein-
499 forced unsaturated polyester. *J Mater Sci* 46:3698–3707. <https://doi.org/10.1007/s10853-010-5136-6>
- 500 29. Ladhar A, Arous M, Kaddami H et al (2017) Correlation between the dielectric and the mechanical
501 behavior of cellulose nanocomposites extracted from the rachis of the date palm tree. In: Paper pre-
502 sented at the IOP conference series: materials science and engineering, vol 258, pp 012001. <https://doi.org/10.1088/1757-899X/258/1/012001>
- 503 30. Chu K, Liu Y, Wang J et al (2018) Oxygen plasma treatment for improving graphene distribution and
504 mechanical properties of graphene/copper composites. *Mater Sci Eng A* 735:398–407. <https://doi.org/10.1016/j.msea.2018.08.064>
- 505 31. Mittal V (2016) Spherical and fibrous filler composites. Wiley, New York, p 8. <https://doi.org/10.1002/9783527670222>
- 506 32. Zhou W, Li T, Yuan M, Li Bo, Dang Z-M (2021) Decoupling of inter-particle polarization and
507 intra-particle polarization in core-shell structured nanocomposites towards improved dielectric per-
508 formance. *Energy Storage Mater* 42:1–11. <https://doi.org/10.1016/j.ensm.2021.07.014>
- 509

511 **Publisher's Note** Springer Nature remains neutral with regard to jurisdictional claims in published
512 maps and institutional affiliations.

513


Journal:	289
Article:	4171

Author Query Form

Please ensure you fill out your response to the queries raised below and return this form along with your corrections

Dear Author

During the process of typesetting your article, the following queries have arisen. Please check your typeset proof carefully against the queries listed below and mark the necessary changes either directly on the proof/online grid or in the 'Author's response' area provided below

Query	Details Required	Author's Response
AQ1	Author details: Kindly check and confirm whether the corresponding author affiliation is correctly identified.	
AQ2	Please update Ref. [11] with volume id and page range, if possible.	